Catalysis Today 145 (2009) 213–219

Contents lists available at ScienceDirect

Catalysis Today

journal homepage: www.elsevier.com/locate/cattod

# Application of high-energy X-rays and Pair-Distribution-Function analysis to nano-scale structural studies in catalysis

Peter J. Chupas [a,*], Karena W. Chapman [a], Hailong Chen [b], Clare P. Grey [b]

[a] X-ray Science Division, Argonne National Laboratory, Argonne, IL 60439, United States
[b] Department of Chemistry, State University of New York at Stony Brook, Stony Brook, NY 11794, United States

ARTICLE INFO

*Article history:*
Available online 1 May 2009

*Keywords:*
Pair-Distribution-Function
High-energy X-rays
Supported catalyst
*In situ* studies

ABSTRACT

We investigate the structure of supported Pt catalysts using high-energy X-ray scattering coupled with Pair-Distribution-Function (PDF) analysis. Recently, experimental approaches that enable the collection of PDF data *in situ* have been developed with time-resolution sufficient to study the structure of Pt nano-particles as they form. The differential PDF approach is utilized which allows the atom–atom correlations involving only Pt to be selectively recovered, enabling structural investigation of the supported particles and the mechanism of their formation. In parallel to the *in situ* analysis, we have examined samples prepared *ex situ*. Data collected on the *ex situ* samples show that the initial deposition of $Pt^{4+}$ occurs as the $PtCl_6^{2-}$ species which are retained even when annealed in an oxygen atmosphere. The Pt differential PDFs of the samples reduced in hydrogen at 200 and 500 °C indicated nano-crystalline face-centered-cubic (fcc) metallic Pt particles. The *ex situ* reduced samples also contain a weak correlations at 2.1 Å, which we assign to Pt–O interactions between the particles and the support surface. The *in situ* experiments, following the reduction of $Pt^{4+}$ from 0 to 227 °C, indicate that the initial Pt nano-particles formed are *ca.* 1 nm in size, and become larger and more crystalline by 200 °C. The data suggest a particle growth mechanism where the initial particles that form are small (<1 nm), then agglomerate into ensembles of many small particles and lastly anneal to form larger well-ordered particles. Lastly, we discus potential future developments in *operando* PDF studies, and identify opportunities for synchronous application of complementary methods.



## 1. Introduction

The development of improved catalyst technology will prove pivotal in meeting the world's future energy demands, wherein more efficient technologies and alternate fuel sources must be exploited [1]. Amongst emergent areas that have been identified for potential development are biomass conversion into liquid fuels [2], fuel-cells that utilize hydrogen in mobile applications [3], and extraction of alternative fossil fuel resources [4]. Implementation of these technologies on commercial scales will require viable heterogeneous catalysts. Significant emphasis has recently been placed on catalyst discovery and synthesis, which has pushed into creation of novel nano-scale architectures [5,6]. However, the realization of rational design of new catalytic concepts and materials will rely on our ability to effectively probe these nano-scale structures. Therefore in addition to the design of new catalysts, new characterization approaches are needed that probe the 1–3 nano-meter scale, and which are amenable to catalyst studies under *in situ* (or *operando*) conditions. Here we describe the application of high-energy X-rays in combination with Pair-Distribution-Function (PDF) analysis to study the structure of supported Pt catalysts, and illustrate the utility of the approach for *in situ* studies.

Supported noble metal catalysts are ubiquitous in industrial applications, most notably in reforming processes, and are potential candidates in new technologies such as fuel-cells. Supported catalysts have been and will continue to be extensively studied by many techniques including X-ray absorption spectroscopy (XAS) [7,8], scanning tunneling microscopy (STM) [9], transmission electron microscopy (TEM) [10], small angle X-ray scattering (SAXS) [11], powder diffraction [12], and NMR [13]. Each of these techniques has its advantages and limitations and often the complexity of the problems in catalysis require a combination of probes for a complete structural picture to be revealed. While microscopy can provide detailed structural information on the nano-meter length-scale, it cannot be used as an *operando* probe of catalyst structure at high temperatures and pressures. XAS, in all its forms (EXAFS, QXAFS, XANES, EDE), form the backbone of the

* Corresponding author at: X-ray Science Division, Argonne National Laboratory, 9700 South Cass Ave., Building 433, Argonne, IL 60439, United States.
Tel.: +1 630 252 8651.
*E-mail address:* chupas@aps.anl.gov (P.J. Chupas).

0920-5861/$ – see front matter © 2009 Elsevier B.V. All rights reserved.
doi:10.1016/j.cattod.2009.03.026

**Table 1**
Sample summary and identification.

| Treatment condition | Sample information (platinum loading given in w/w) | | | |
|---|---|---|---|---|
| | $TiO_2$ | 2.5% Pt on $TiO_2$ | 5.0% Pt on $TiO_2$ | 7.5% Pt on $TiO_2$ |
| 60 °C/overnight/air | $TiO_2$/60 °C | 2.5%Pt/60 °C | 5%Pt/60 °C | 7.5%Pt/60 °C |
| 200 °C/2 h/$O_2$ | $TiO_2/O_2$200 °C | 2.5%Pt/$O_2$200 °C | 5%Pt/$O_2$200 °C | 7.5%Pt/$O_2$200 °C |
| 200 °C/2 h/$H_2$ | $TiO_2/H_2$200 °C | 2.5%Pt/$H_2$200 °C | 5%Pt/$H_2$200 °C | 7.5%Pt/$H_2$200 °C |
| 500 °C/5 h/$H_2$ | $TiO_2/H_2$500 °C | 2.5%Pt/$H_2$500 °C | 5%Pt/$H_2$500 °C | 7.5%Pt/$H_2$500 °C |

experimental methodology used for studying catalyst structure, though its limitation lies in the fact is does not probe distances longer than ~5 Å. NMR, while a powerful local structural probe, is limited primarily to *ex situ* studies. Small angle X-ray scattering (SAXS) does access nano-meter length-scales and allow the shape and size of particles to be investigated, however it does not yield structural detail with atomic scale resolution, which is often crucial in unraveling catalytic mechanisms. However, the Pair-Distribution-Function (PDF) method that can deliver atomic resolution structural information similar to EXAFS, but which extends to distances of several nanometers, and thus fills an important gap left by the mainstream structural probes [14].

The PDF technique recovers structural information in the form of a radial distribution function of inter-atomic distances [14]. PDF analysis has already proven itself a powerful technique for the analysis of nano-crystalline materials [14], including both local structural information and intermediate range order (10–20 Å), and has even been applied to a variety of systems in catalysis, including supported metal catalysts [15,16], zeolites [17,18], alumina acid catalysts [19,20], and more recently ceria [21]. Only recently with major instrumental advances and the availability of high-energy X-rays at high energy third-generation synchrotrons, have *in situ* or *operando* PDF studies been made possible. Previously, such *in situ* studies were impractical because of the prohibitively long data collection times, typically measured in days or weeks. Our work, in adapting area detectors to PDF measurements and coupling them to the large fluxes high-energy X-rays available at third-generation synchrotrons, has demonstrated time-resolved PDF studies with resolution down to 30 ms [16,22–24]. With fast-time-resolution that rivals that possible with energy dispersive EXAFS [8], *in situ* PDF studies in catalysis are now possible, allowing both local and long-range structure to be directly probed.

Previously we reported a quantitative kinetic analysis of the reduction of $Pt^{4+}$ on $TiO_2$ using time-resolved PDF methods [16]. Here we extend these studies of $TiO_2$ supported Pt to probe the structure of the platinum particles and follow the structural changes that occur during their formation. We use both *ex situ* and *in situ* differential PDF (d-PDF) methods, which in the case of supported catalysts allows the selective recovery of atom–atom correlations arising only from the supported clusters (i.e. Pt–Pt and Pt–X contacts are recovered). We demonstrate that the initial formation of $Pt^0$ yields a material with good structural coherence over a length-scale of 1.0 nm, which, on further annealing forms larger particles of metallic Pt with increased crystallinity.

## 2. Experimental

### 2.1. Materials preparation

$H_2PtCl_6$, Pt, $PtO_2$ and $TiO_2$ were obtained from Aldrich, and gases were obtained from BOC gas. Samples of 2.50% (w/w), 5.00% (w/w) and 7.50% (w/w) of Pt metal on $TiO_2$ were prepared using $H_2PtCl_6$ as a precursor and each of the initial series of samples were made starting with approximately 5 g $TiO_2$. Samples with different loadings of platinum were made using aqueous impregnation methods and dried at 60 °C overnight. The samples are labeled as follows: $TiO_2$/60 °C, 2.5%Pt/60 °C, 5.0%Pt/60 °C, and 7.5%Pt/60 °C. Approximately, 1.0 g from each of the /60 °C samples was then calcined at 200 °C for 2 h under a flow of oxygen. These samples are labeled $TiO_2/O_2$200 °C, 2.5%Pt/$O_2$200 °C, 5.0%Pt/$O_2$200 °C, and 7.5%Pt/$O_2$200 °C. An additional ~1.0 g sample from each of the /60 °C samples was then treated at 200 °C for 2 h under a flow of 5%$H_2$ in argon. These samples are labeled $TiO_2/H_2$200 °C, 2.5%Pt/$H_2$200 °C, 5.0%Pt/$H_2$200 °C, and 7.5%Pt/$H_2$200 °C. Lastly, a 1.0 g sample from each of the /60 °C samples was then treated at 500 °C for 5 h under a flow of 5%$H_2$ in argon. These samples were labeled $TiO_2/H_2$500 °C, 2.5%Pt/$H_2$500 °C, 5.0%Pt/$H_2$500 °C, and 7.5%Pt/$H_2$500 °C. See Table 1 for a summary of sample composition, treatment and names.

### 2.2. TEM

As a typical sample preparation procedure, about 0.2 mg of sample was put in 10 ml absolute ethyl alcohol and was sonicated in a ultrasonic bath for 5 min to achieve good dispersion. One drop of the solution was dropped on a lacey carbon coated 400 mesh copper grid and dried in air. The images were taken under a Philips CM12 scanning transmission electron microscope using a 120 kV acceleration voltage at various magnifications.

### 2.3. Details of the diffraction experiments

Diffraction experiments were performed at the 11-ID-B beamline at the Advanced Photon Source (APS) located at Argonne National Laboratory, Argonne, Illinois (USA). X-rays with a wavelength of 0.2128 Å were used for the experiments. This wavelength was selected to be below the Pt K adsorption edge to minimize sample fluorescence. A Mar345 image plate mounted orthogonal to the beam path was used for the experiments. A $CeO_2$ standard and the software Fit2D [25] were used to calibrate the image plate as previously described. Combining high-energy X-rays and a relatively short sample detector distance (~15 cm) allow access to a large $Q_{max}$ of ~25.0 $Å^{-1}$. For the time-resolved experiments a sample of 5.0%Pt/60 °C was assembled into a previously described reaction cell that allows gas flow [26,27]. The sample was cooled to 0 °C under helium flow using an Oxford Cryosystems Cryostream 700 Plus. The gas flow was switched to 100% hydrogen, and the temperature was then ramped from 0 to 227 °C over 2 h. This procedure was repeated for the $TiO_2$ support material. All data were integrated using the software Fit2D [25] and converted to intensity versus scattering angle. Data were corrected for distortions in intensity due to angle of incidence of the diffracted beam, sample absorption, multiple scattering, polarization, Laue diffuse scattering and Compton scattering to obtain the reduced structure function $F(Q)$ as previously described [24] using the program PDFgetX2 [28]. Direct Fourier transform of $F(Q)$ yields the experimental PDF $G(r)$. Fitting of models to the experimental PDFs was performed using the program PDFFIT [29].

### 2.4. Details of the PDF technique

The atomic Pair-Distribution-Function (PDF), $G(r)$, is defined as:

$$G(r) = 4\pi r[\rho(r) - \rho_0] \quad (1)$$

The terms $\rho(r)$ and $\rho_0$ are the local and average atomic number densities, respectively, and $r$ is the radial distance. The term for local atomic number density, $\rho(r)$, can be expanded to $\rho_0 g(r)$, where $g(r)$ is a direct measure of the probability of finding two atoms at a distance $r$. The strength of using the definition, $G(r)$, is that it is obtained directly obtained by Fourier transformation of the total structure function $S(Q)$. Obtaining $g(r)$ requires knowledge of the density of the materials under study. The measurable quantity, $S(Q)$, is defined as a function of $Q$, the magnitude of the wave-vector ($Q = 4\pi \sin(\theta)/\lambda$).

$$S(Q) = 1 + \left[\frac{I^{\mathrm{coh}}(Q) - \sum c_i |f_i(Q)|^2}{|\sum c_i f_i(Q)^2|}\right] \quad (2)$$

$I^{\mathrm{coh}}(Q)$ is the coherent scattering intensity per atom in electron units. The terms $c_i$ and $f_i$ are the atomic concentration and scattering form factors for atom type $i$, respectively. It is important to note here that the function, $S(Q)$, is continuous over $Q$. Therefore, it measures all scattering intensity, both the Bragg and diffuse components. The PDF, $G(r)$, can be determined by direct Fourier transform, over the entire measured $Q$ range.

$$G(r) = \frac{2}{\pi}\int Q[S(Q) - 1]\sin(Qr)\,dQ \quad (3)$$

The PDF provides information regarding local atomic structure. The resolution of the PDF is determined in large part by the magnitude of the $Q$ range covered.

## 3. Results and discussion

Quantitative d-PDF analysis on heterogeneous catalysts requires that the contributions from the support can be accurately subtracted from the total PDF to yield a d-PDF that contains only atom–atom correlations from the supported particles. Thus, any changes in the structure of the support during chemical and/or thermal treatment need to be quantified. To ensure that there are no artifacts in the d-PDF, we first measure the PDFs of the $TiO_2$ samples to guarantee that the support was not changing during the experimental conditions we investigated. Diffraction data was obtained for the titania samples $TiO_2$/60 °C, $TiO_2/O_2$200 °C, $TiO_2/H_2$200 °C, and $TiO_2/H_2$500 °C. PDFs were obtained from the diffraction data and those obtained for $TiO_2$/sm and $TiO_2/H_2$500 °C are shown in Fig. 1, and are identical to within statistical errors. The diffraction data show that the $TiO_2$ samples are purely the anatase form, and that the treatments yielded no discernable changes in the structure as a function of treatment conditions.

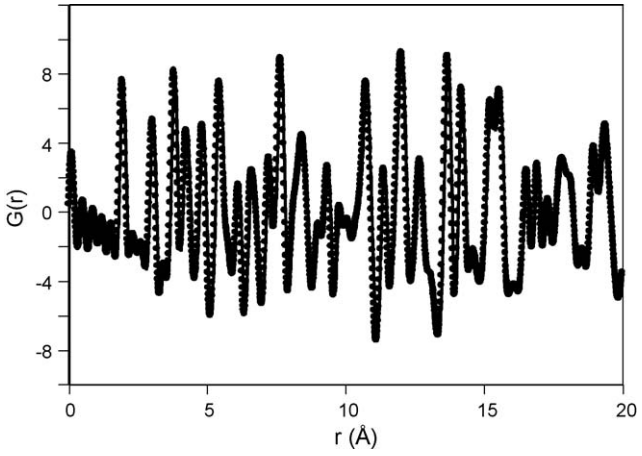


**Fig. 1.** The experimentally determined PDFs, $G(r)$, for $TiO_2$/60 (black line) and $TiO_2/H_2$500 (black circles).

The TEM micrograph in Fig. 2 shows sample 5%Pt/$H_2$200 °C. Particles of Pt are evident on the $TiO_2$ support, and it is easy to identify both isolated small particles and larger agglomerates. Utilizing the d-PDF approach we are able to isolate atomic resolution structural information from only the Pt component of the samples. An example of a differential PDF on sample 2.5%Pt/$H_2$200 °C is shown in Fig. 2. Fig. 2a shows both the PDF of the support ($TiO_2/H_2$200 °C) (grey line) and the PDF of sample 2.5%Pt/$H_2$200 °C (black line). The d-PDF (i.e. $G(r)_{2.5\%\mathrm{Pt}/H_2200\,^\circ\mathrm{C}} - G(r)_{TiO_2/H_2200\,^\circ\mathrm{C}}$) is shown in Fig. 2a. The d-PDF contains only atom–atom correlations involving platinum, which potentially include Pt–Pt, Pt–Cl, Pt–O, and Pt–Ti.

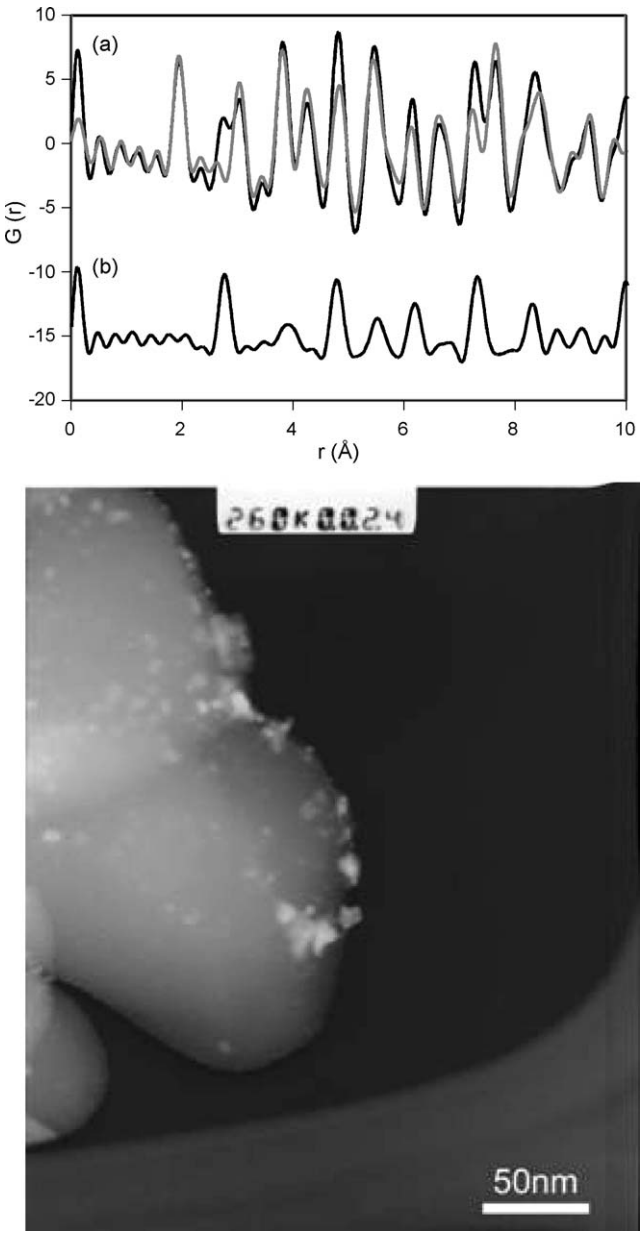


**Fig. 2.** An example of a differential PDF. (a) The grey line is the measured $G(r)$ for $TiO_2$ while the black line is the measured $G(r)$ for a 2.5% Pt on $TiO_2$ calcined under a flow of 5% $H_2$ in Argon. (b) The differential PDF calculated between the two measured PDFs, $G(r)_{2.5\%\mathrm{Pt}/TiO_2} - G(r)_{TiO_2}$. (Bottom) TEM micrograph of sample 5.0%Pt/$H_2$200.

Unlike EXAFS, the method is not limited to the first few coordination shells, and can allow a length-scale as far as 4–5 nm to be probed, in principle allowing the size of a nano-particle to be investigated [30]. This length-scale covers the entire particle dimensions of most supported catalysts.

To assess the effect of the Pt loading level and estimate the level needed for time-resolved experiments, a series of *ex situ* prepared samples were investigated. All the PDFs on the *ex situ* prepared samples were collected with a single image from the area detector as a direct analogy to the way data would be collected in a time-resolved experiment. With regards to image-plate (IP) technology the ultimate time resolution of the experiment is largely governed by the time it takes to read out the detector (~1–2 min), though currently area detectors with faster readout are available [23]. The overall sensitivity of the measurements is dictated by the dynamic range and efficiency of the detector, though with faster readout detectors significant increases in signal-to-noise is possible by averaging hundreds or even thousands of individual images over minutes to hours [31]. Fig. 3 shows the differential PDFs determined for 2.5%Pt/60 °C, 5.0%Pt/60 °C, and 7.5%Pt/60 °C. There is a clear correlation that grows in magnitude on platinum loading at ~2.35 Å. The measured distance is absolute and is not associated with an offset, or dependent on a model, as is typically the case for distances measured from EXAFS experiment. As expected, this distance is shorter than would be expected for metallic Pt and could therefore be indicative of either $Pt^{4+}$–Cl or $Pt^{4+}$–O correlations. However, based on bond lengths determined from the PDFs of $PtO_2$ and $H_2PtCl_6$ (shown at the bottom of Fig. 4) we assign this correlation to be Pt–Cl. The lack of well defined correlations in the differential $G(r)$s at distances longer than 5 Å indicates the lack of a periodically ordered long-range structure beyond these distances. Thus, it is clear that the deposition of the initial $Pt^{4+}$ occurs as a phase lacking long-range order with platinum occurring as molecular $PtCl_6^+$. A second weaker correlation is evident at ~3.35 Å and can be attributed to Cl–Cl correlations of the $PtCl_6$ octahedra. While the Pt–Cl correlation is clearly evident in the $G(r)$ of the 2.5%Pt/60 °C sample, there is a non-negligible contribution from statistical noise and termination ripples, thus the *in situ* experiments described later utilize a higher loading of platinum (5%).

The differential PDFs of 2.5%Pt/$H_2$200 °C, 5.0%Pt/$H_2$200 °C, 7.5%Pt/$H_2$200 °C, 2.5%Pt/$H_2$500 °C, 5.0%Pt/$H_2$500 °C, and 7.5%Pt/

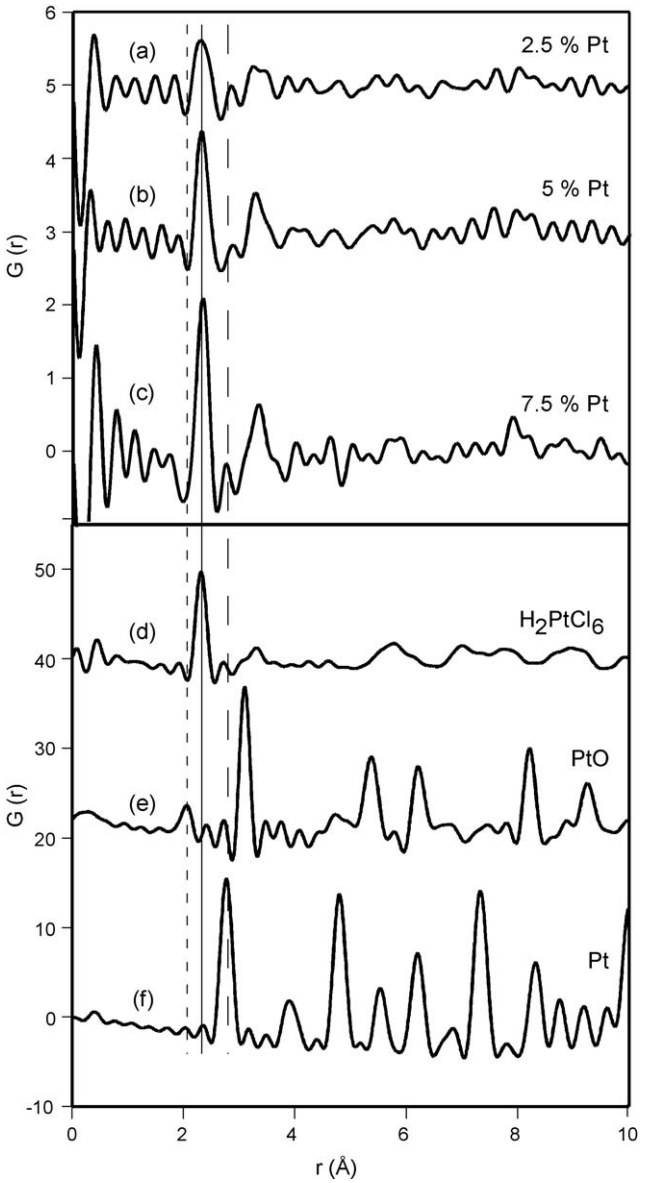


**Fig. 3.** The differential PDFs for (a) 2.5%Pt/60, (b) 5.0%Pt/60, and (c) 7.5%Pt/60. $G(r)$s of (d) $H_2PtCl_6$, (e) $PtO_2$ and (f) Pt are shown for comparison.

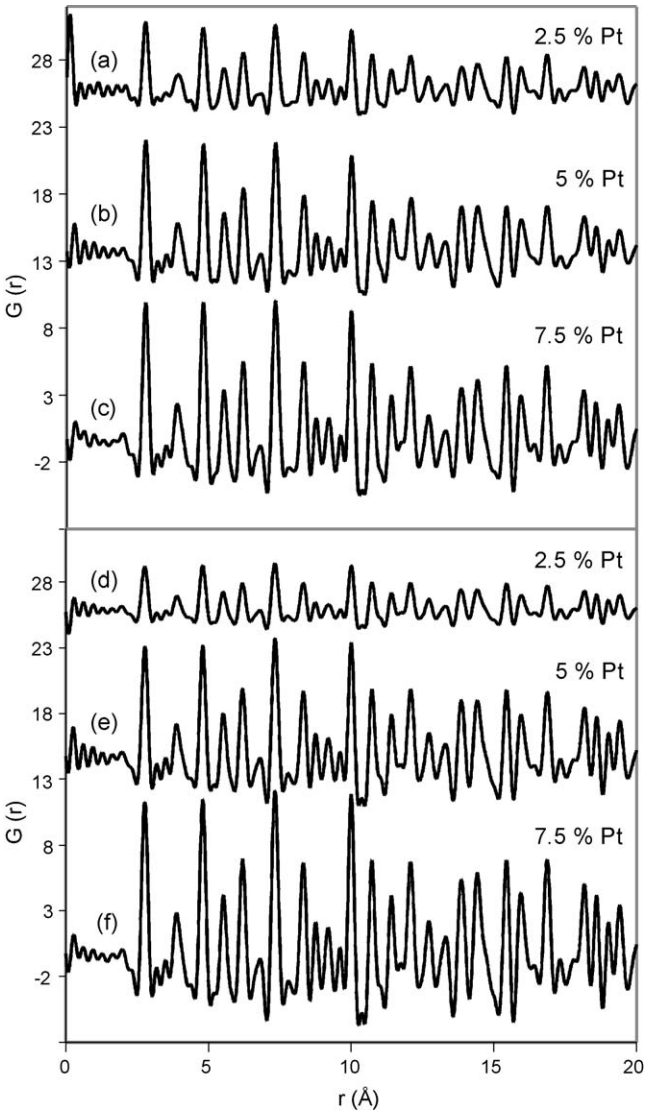


**Fig. 4.** The differential PDFs for (a) 2.5%Pt/$H_2$200, (b) 5.0%Pt/$H_2$200, (c) 7.5%Pt/$H_2$200, (d) 2.5%Pt/$H_2$500, (e) 5.0%Pt/$H_2$500, and (f) 7.5%Pt/$H_2$500.

$H_2$500 °C are shown in Fig. 4. Clearly metallic Pt particles have formed as a result of reduction of $Pt^{4+}$ with treatment under a reducing atmosphere of hydrogen. The reduction of Pt at 500 °C versus 200 °C leads to larger and more crystalline particles. This is evidenced by the fact that sharper more intense correlations are evident above 10 Å in the PDF of the samples treated at 500 °C. This behavior is indicative of sintering of the Pt particles, and is consistent with SAXS measurements examining thermal treatment of Pt on $SiO_2$ [11]. In both sets of samples a weak correlation at 2.1 Å is noticeable, particularly in the higher loadings of Pt. We assign this correlation to Pt–O based on bond length, which is an expected to be interaction of the particles with the surface of the support. This distance is longer than the Ti–O distance of ~2.0 Å and is unlikely to be an artifact from the subtraction procedure. The resolution of the PDFs reported would readily distinguish correlations separated by 0.1 Å.

PDFs obtained from the *in situ* experimental diffraction data are shown in Fig. 6. These PDFs contain all the atom–atom correlations in the sample, including those from both the $TiO_2$ support and the deposited $Pt^{4+}$ salt. The first correlation at ~2 Å, which shows no significant change in intensity during the reduction (see Fig. 5a), corresponds to the first Ti–O coordination shell, while the weak peak at 2.5 Å, which decreases markedly in intensity during reduction, corresponds to the consumption of Pt–Cl bonds.

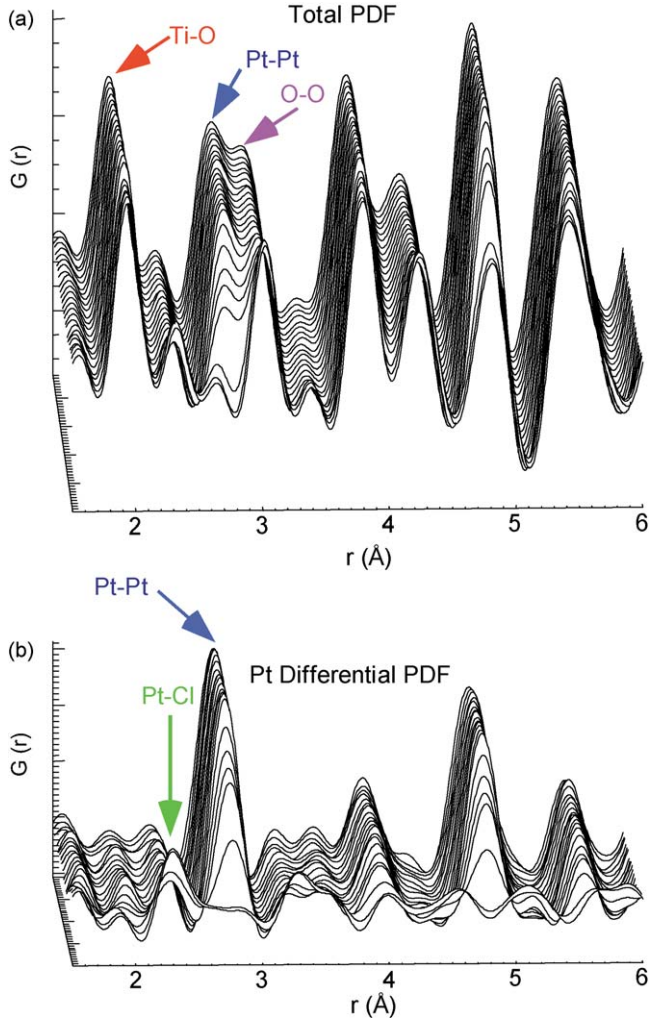


**Fig. 5.** (a) The total PDFs for 5% (w/w) Pt on $TiO_2$ reduced under $H_2$ from 0 to 227 °C over 2 h. (b) The differential PDFs containing only atom–atom correlations involving Pt.

The Pt differential PDFs (Fig. 5b) were determined by direct subtraction of the PDF of the bare support, $TiO_2$, from the PDF of the platinum supported material, after renormalization of the PDFs to the Ti–O correlation (at ~2.0 Å). Care was taken to ensure that both data sets, the total PDF and reference $TiO_2$ PDF, were acquired at the same temperature. The d-PDF of the pristine material is dominated by two peaks at ~2.35 Å (Pt–Cl bonds) and ~3.35 Å. The peak at ~2.8 Å, which develops very rapidly on heating, corresponds to the first shell Pt–Pt first coordination bond length. The d-PDF of the *ex situ* sample (Fig. 2a) illustrates the extended length-scales to which structural information can be derived.

Fig. 6a shows the integrated intensities of the two Pt–Pt correlations at ~2.8 and ~8.5 Å. Three distinct regions are observed. From 0 to 20 °C the intensity of the Pt–Pt correlations increases rapidly corresponding to the reduction of Pt(IV) and the formation of metallic Pt particles. Even in this regime, the two Pt contacts grow at a similar rate (within the errors of the measurements), indicating that the Pt particles that have formed are larger than 8.5 Å following only 2 min of reaction (the 1st data point). This intensity increase is associated with a large loss in the Pt–Cl contacts, the $Cl^-$ presumably being lost as HCl. The intensity

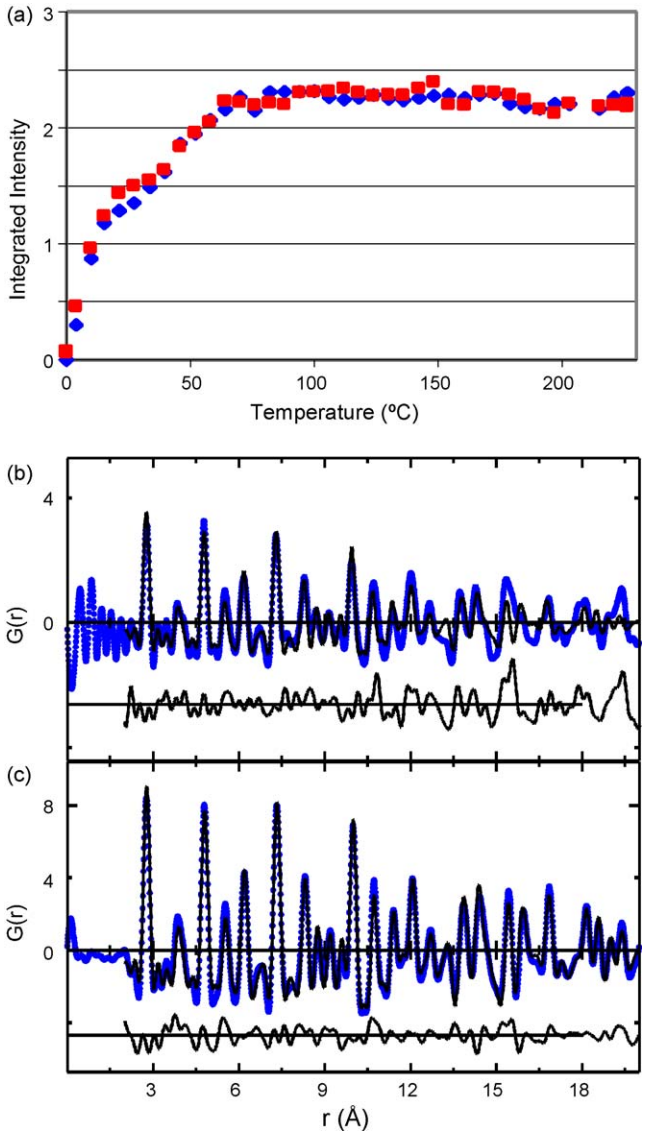


**Fig. 6.** (a) The integrated peak intensity of the Pt–Pt correlations at ~2.8 Å (diamonds) and ~8.5 Å (squares). The refinement of the data for (b) *in situ*/58 °C and (c) *ex situ*/200 °C over the range of 2–20 Å.

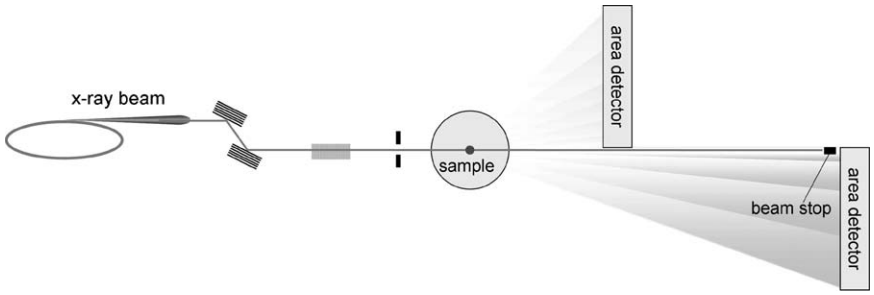


**Fig. 7.** Example of a setup that would enable the collection of both SAXS and PDF data. For example, working at a wavelength of 0.2 Å it would be possible to collect both PDF data ($Q_{max}$ ~30 Å$^{-1}$) and SAXS data with a $Q_{min}$ of 0.01 Å.

increases at a slower rate from 20 to 70 °C, which is possibly due to further reduction of $Pt^{4+}$ species, annealing of defects, or the increase of average particle size. Lastly, above 70 °C no changes in the intensity are evident. Differences in the ratio of intensities of the two correlations would be expected if significant changes in particle size or crystallinity were occurring. Differences in these correlations are evident when the sample is annealed at high temperatures, for example in comparing 5%Pt/$H_2$200 °C and 5%Pt/$H_2$500 °C.

The d-PDFs of the *in situ* data at 58 °C (*in situ*/58 °C), the *in situ* data at 227 °C (*in situ*/227 °C), and the samples 5%Pt/$H_2$200 °C and 5%Pt/$H_2$500 °C were used to refine the structure, using fcc Pt structure as a starting model. The data used in the refinement were varied from $r_{min}$ of 2.0 Å to a $r_{max}$ of from 8 to 24 Å in order to probe particle sizes. For crystalline materials, the weighted profile agreement factors ($R_{wp}$s) are not weighted by the data range. The fit to the data in the region from 10 to 20 Å is significantly worse for *in situ*/58 °C sample versus 5%Pt/$H_2$200 °C (Fig. 6b and c). When refined over the range from 2 to 10 Å, the refinements yielded comparable $R_{wps}$ (weighted profile agreement factor) of 21.3, 17.7, and 16.8 for *in situ*/227 °C, 5%Pt/$H_2$200 °C, and 5%Pt/$H_2$500 °C, respectively and a slightly larger $R_{wp}$ of 25.7 for *in situ*/58 °C. When the range of the refinements was expanded to the range from 2 to 20 Å, the $R_{wp}$s obtained for the *in situ* samples increased noticeably and values of 46.2, 31.0, 18.7, and 18.5 were obtained for *in situ*/58 °C, *in situ*/227 °C, 5%Pt/$H_2$200 °C, and 5%Pt/$H_2$500 °C, respectively.

These results indicate that the reduction of $Pt^{4+}$ at low temperatures (<60 °C) yields "crystallites" with a well-ordered face-centered-cubic (fcc) structure over a length-scale of 8 Å, as observed in the d-PDF of *in situ*/58 °C. Annealing/sintering of the samples over either prolonged periods at moderate temperatures (~200 °C) or treatment at higher temperatures (~500 °C) yield more samples with higher crystallinity and larger (>3 nm) particle sizes.

## 4. Conclusion and future outlook

Using PDF analysis we have been able to examine the atomic resolution structure of supported Pt nano-particles both on samples treated *ex situ* and on transformations occurring under *in situ* conditions. We show that $Pt^{4+}$ is deposited as $PtCl_6^{2-}$ species which are retained even when annealed in oxygen. Samples of $Pt^{4+}$ reduced *ex situ* under hydrogen yield materials with metallic face-centered-cubic platinum particles. Examining the d-PDFs of the reduced samples with various Pt loading, a weak correlation develops at 2.1 Å, which we assign to Pt–O interactions between the particles and the surface of the support. The *in situ* experiments were used to follow the reduction or $Pt^{4+}$ from 0 to 227 °C and examine the mechanism of particle formation. The initial Pt nano-particles that form are ~1 nm in size, while by 200 °C are larger and more crystalline. This suggests a mechanism for particle growth where the initial particles that form are small (<1 nm) then agglomerate into ensembles of many small particles and lastly anneal to form larger well-ordered particles. In conclusion, we have demonstrated how the PDF technique can be applied to studies in catalysis.

The trend and future direction of structural studies in catalysis is in probing active materials at different length-scales and will require the combination of multiple probes as well as adapting them for *in situ* or *operando* studies. PDF is well suited to *operando* studies as it utilizes high-energy X-rays which are highly penetrating and which allow a great degree of flexibility in the design of reaction cells. One weakness in PDF is the difficulty in analyzing particle shape, which is exacerbated with many real samples in that a dispersion of particle sizes/shapes are present. In the future, the combination of PDF with a probe, such as SAXS, seems warranted. SAXS is well suited to probing nano-meter scale structure, particularly at lengths comparable to the atomic scale resolution obtained from PDF. For example, Fig. 7 shows a layout that would allow both high-resolution ($Q_{max}$ ~ 30 Å$^{-1}$) and SAXS measurements ($Q_{min}$ ~ 0.01 Å$^{-1}$) to be collected, using a reasonable camera length (~5 m) for the later. This would enable a simultaneous probe of both particle size and shape and allow atomic-scale resolution structure to be probed.

## Acknowledgements

This work was supported through grant DE-FG02-96ER14681 from the U.S. DOE. Work performed at Argonne National Laboratory was supported by the U.S. DOE, Office of Science, Office of Basic Energy Sciences, under Contract No. DE-AC02-06CH11357.

## References

[1] A.T. Bell, B.C. Gates, D. Ray, Basic Research Needs: Catalysis for Energy, Report from the U.S. Department of Energy Basic Energy Sciences Workshop, August 6–8, 2007.
[2] G.W. Huber, J.N. Chheda, C.J. Barrett, J.A. Dumesic, Science 308 (2005) 1446.
[3] B.C.H. Steele, A. Heinzel, Nature 414 (2001) 345.
[4] A. Andrews, Oil Shale: History, Incentives and Policy; Congress Research Service, The Library of Congress, Washington, DC, 2006, RL33359.
[5] A.T. Bell, Science 299 (2003) 1688.
[6] D.R. Rolison, Science 299 (2003) 1698.
[7] A.M. Argo, J.F. Goellner, B.L. Phillips, G.A. Panjabi, B.C. Gates, J. Am. Chem. Soc. 123 (2001) 2275.
[8] M.A. Newton, A.J. Dent, J. Evans, Chem. Soc. Rev. 31 (2002) 83.
[9] O. Dulub, W. Hebenstreit, U. Diebold, Phys. Rev. Lett. 84 (2000) 3646.
[10] J.M. Thomas, P.A. Midgley, Chem. Commun. 11 (2004) 1253.
[11] R.E. Winans, S. Vajda, B. Lee, S.J. Riley, S. Seifert, G.Y. Tikhonov, N.A. Tomczyk, J. Phys. Chem. B 108 (2004) 18105.
[12] M. Fernandez-Garcia, A. Martinez-Arias, J.C. Hanson, J.A. Rodriguez, Chem. Rev. 104 (2004) 4063.
[13] H.E. Rhodes, P. Wang, H.T. Stokes, C.P. Slichter, J.H. Sinfelt, Phys. Rev. B 26 (1982) 3559.
[14] T. Egami, S.J.L. Billinge, in: R. Cahn (Ed.), Underneath the Bragg Peaks: Structure Analysis of Complex Materials, Oxford/Pergamon Press, New York, 2004.
[15] P. Gallezot, G. Bergeret, J. Catal. 72 (1981) 294.
[16] P.J. Chupas, K.W. Chapman, G. Jennings, P.L. Lee, C.P. Grey, J. Am. Chem. Soc. 129 (2007) 13822.

[17] R.D. Shannon, G. Bergeret, P. Gallezot, Nature 215 (1985) 736.
[18] R.D. Shannon, K.H. Gardner, R.H. Staley, G. Bergeret, P. Gallezot, A. Aurouz, J. Phys. Chem. 89 (1985) 4778.
[19] G. Paglia, E. Bozin, S.J.L. Billinge, Chem. Mater. 18 (2006) 3242–3248.
[20] P. Ratnasamy, A.J. Leonard, Catal. Rev. 6 (1972) 293.
[21] E. Mamontov, T. Egami, J. Phys. Chem. Solids 61 (2000) 1345.
[22] P.J. Chupas, X. Qiu, P.L. Lee, J.C. Hanson, C.P. Grey, S.J.L. Billinge, J. Appl. Crystallogr. 36 (2003) 1342.
[23] P.J. Chupas, K.W. Chapman, P.L. Lee, J. Appl. Crystallogr. 40 (2007) 463.
[24] P.J. Chupas, S. Chaudhuri, J.C. Hanson, X. Qiu, P.L. Lee, S.D. Shastri, S.J.L. Billinge, C.P. Grey, J. Am. Chem. Soc. 126 (2004) 4756.
[25] A.P. Hammersley, S.O. Svenson, M. Hanfland, D. Hauserman, High Pressure Res. 14 (1996) 235.
[26] P.J. Chupas, K.W. Chapman, C. Kurtz, J.C. Hanson, P.L. Lee, C.P. Grey, J. Appl. Crystallogr. 41 (2008) 822.
[27] P.J. Chupas, M.F. Ciraolo, J.C. Hanson, C.P. Grey, J. Am. Chem. Soc. 123 (2001) 1694.
[28] X. Qiu, J.W. Thompson, S.J.L. Billinge, J. Appl. Crystallogr. 37 (2004) 678.
[29] T. Proffen, S.J.L. Billinge, J. Appl. Crystallogr. 32 (1999) 572.
[30] K. Page, T. Proffen, H. Terrones, M. Terrones, L. Lee, Y. Yang, S. Stemmer, R. Seshadri, A.K. Cheetham, Chem. Phys. Lett. 393 (2004) 385.
[31] K.W. Chapman, P.J. Chupas, E.R. Maxey, J.W. Richardson, Chem. Commun. (2006) 4013.